

Two-dimensional non-Hermitian Skin Effect in a Synthetic Photonic Lattice

Yiling Song,¹ Weiwei Liu,^{1,*} Lingzhi Zheng,¹ Yicong Zhang,¹ Bing Wang^{1,†} and Peixiang Lu^{1,2}

¹Wuhan National Laboratory for Optoelectronics and School of Physics, Huazhong University of Science and Technology, Wuhan 430074, China

²Hubei Key Laboratory of Optical Information and Pattern Recognition, Wuhan Institute of Technology, Wuhan, 430205, China



(Received 13 October 2020; revised 30 November 2020; accepted 8 December 2020; published 30 December 2020)

Non-Hermitian skin effect (NHSE) has led to interesting physics and sophisticated applications beyond the conventional framework. However, NHSE studies have been limited to an individual dimension due to the difficulty of constructing nonreciprocal coupling in higher-dimensional systems. With the concept of synthetic dimension, we realize two-dimensional (2D) NHSE in a synthetic photonic lattice. The synthetic photonic lattice is composed of a spatial dimension and a synthetic frequency dimension, which is constructed by introducing gain and loss and dynamically modulating the complex refractive index in a one-dimensional ring-resonator array. In the synthetic 2D NHSE system, we can manipulate the spatial position and frequency mode of the light in real time, thus enabling programmable light propagation and frequency conversion. Specifically, the incident light can be localized in the spatial dimension and the frequency dimension simultaneously, leading to second-order corner modes in the synthetic 2D NHSE lattice. Besides, the 2D NHSE system exhibits an excellent robustness for the disorder and point defect in the lattice. This work generalizes the non-Hermitian skin effect in synthetic dimension to control the light in different dimensions, which shows great promise for potential applications in on-chip light manipulation, frequency synthesis, and information processing.

DOI: 10.1103/PhysRevApplied.14.064076

I. INTRODUCTION

Non-Hermitian Hamiltonians provide a powerful tool for describing the interaction between a system and the surroundings [1–7]. As a consequence, non-Hermitian systems have been widely studied in a variety of fields, such as quantum mechanics [8,9], condensed-matter physics [10,11], and optics [12–14], both in theory and experiments. Generally, non-Hermitian systems can be realized by judiciously introducing gain and loss [15–17]. Non-Hermitian skin effect (NHSE), one of the most remarkable phenomena in non-Hermitian systems, has attracted great attention [13,18–22]. Under an open-boundary condition (OBC), the anisotropic couplings between the adjacent sites force the majority of the eigenstates to be localized at the boundaries of the non-Hermitian systems [23–25]. This feature suggests attractive physics of the NHSE in classical and quantum systems. For example, the NHSE leads to the breakdown of the conventional bulk-boundary correspondence, suggesting a completely different principle for understanding the non-Hermitian topological properties in open systems [18,19,26–28]. More recently, the NHSE has

been utilized to steer the light flow in a photonic mesh system and provide a highly efficient funnel for light [13].

High-dimensional non-Hermitian systems allow vast and flexible settings for studying the interaction between electromagnetic wave propagation and the environment [29–31]. However, the NHSE is usually realized in an individual physical dimension, because the difficulty for constructing nonreciprocal coupling in different dimensions has prevented the development of the NHSE in high-dimension systems. Fortunately, the concept of synthetic dimension has brought a versatile solution for exploring high-dimensional physics [32–40]. In optics, synthetic dimensions have been created by frequency modes [33–35], orbital angular momentum [36,37], and multiple pulses [38,39], showing great promise for realizing rich optical and photonic effects in virtual dimensions. Therefore, taking advantage of the synthetic dimension, the NHSE can be investigated in a higher-dimensional non-Hermitian system consisting of both real and virtual dimensions simultaneously.

Here, we realize the two-dimensional (2D) NHSE in a synthetic photonic lattice composed by a spatial dimension and a synthetic frequency dimension. Firstly, we construct an array of ring resonators with anisotropic coupling to obtain a one-dimensional (1D) NHSE system in spatial

*lwhust@hust.edu.cn

†wangbing@hust.edu.cn

dimension. Then, as the ring resonator possesses a series of discrete frequency modes, a 2D photonic lattice can be formed by stacking the resonators in a synthetic ladder along the frequency dimension [41,42]. The longitudinal coupling between the frequency modes is driven by a dynamic modulation of the complex refractive index of the ring-resonator array. Specifically, by controlling the isotropic and anisotropic coupling in the frequency dimension, the first-order and second-order non-Hermitian skin effects can be, respectively, realized in the synthetic 2D photonic lattice. Thanks to the flexibility of the synthetic NHSE system, we can manipulate the position and frequency mode of the light in real time, which enables programmable light propagation and frequency conversion. Besides, the 2D NHSE system exhibits excellent robustness for the disorder and point defect in the synthetic lattice.

II. RESULTS AND DISCUSSION

To construct a photonic lattice with anisotropic coupling in real space, gain and loss are introduced into an array

composed of ring resonators, as illustrated in Fig. 1(a). The gray rings and the red-green rings represent the on-site rings and the link rings, respectively. The size of the on-site rings is designed to satisfy the resonance condition. Here, we focus on the counterclockwise modes in the on-site rings. The coupling from left to right occurs by passing through the upper part of the link ring (red arrow), which represents a gain process. In contrast, the coupling in the opposite direction is through the lower part (green arrow), which represents a loss process. As a consequence, the lattice can be equivalent to a 1D chain with anisotropic coupling between the adjacent sites [43], as shown in Fig. 1(b). The system can be described by the Hatano-Nelson model, which exhibits the first-order skin effect, and the non-Hermitian Hamiltonian is expressed as [19,22,44,45]

$$H = \sum_n (\kappa + \delta) a_{n+1}^\dagger a_n + (\kappa - \delta) a_n^\dagger a_{n+1}, \quad (1)$$

where a_n^\dagger (a_n) is the creation (annihilation) operator of the n th on-site ring. κ is the isotropic coupling strength

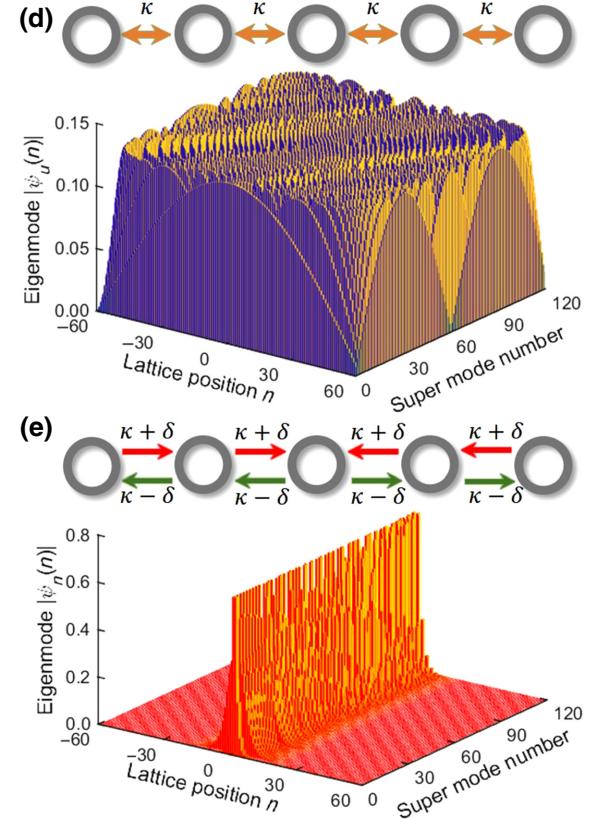
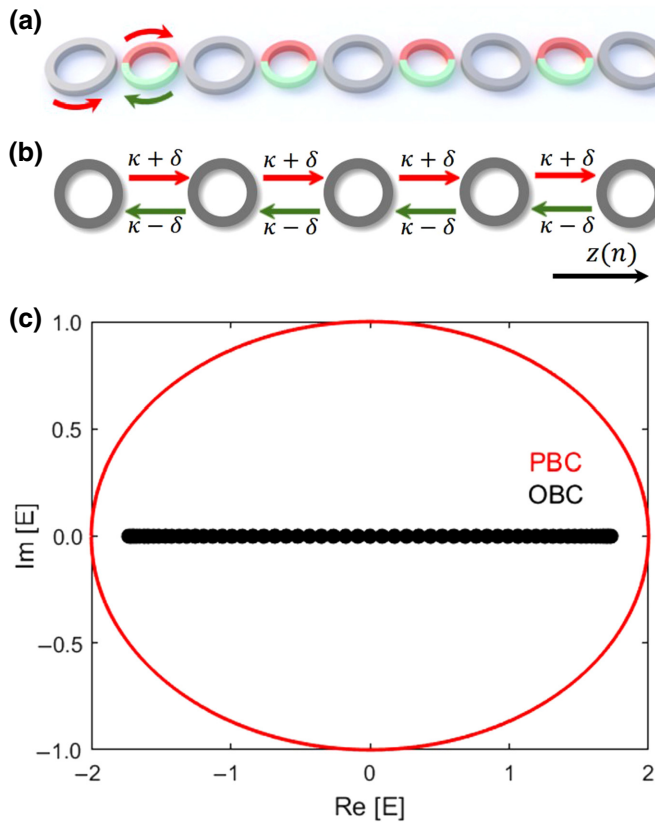


FIG. 1. 1D non-Hermitian skin effect in spatial dimension. (a) Scheme of the structure for the 1D NHSE model. The red part and green part represent gain and loss mediums, respectively. (b) Schematic diagram for the 1D NHSE model. (c) Calculated eigenenergy for the OBC (black spots) and PBC (red line), respectively. (d) A 1D lattice composed of isotropically coupled ring resonators (120 sites), and the calculated eigenmodes. (e) A 1D lattice composed of anisotropically coupled ring resonators (120 sites), and the calculated eigenmodes.

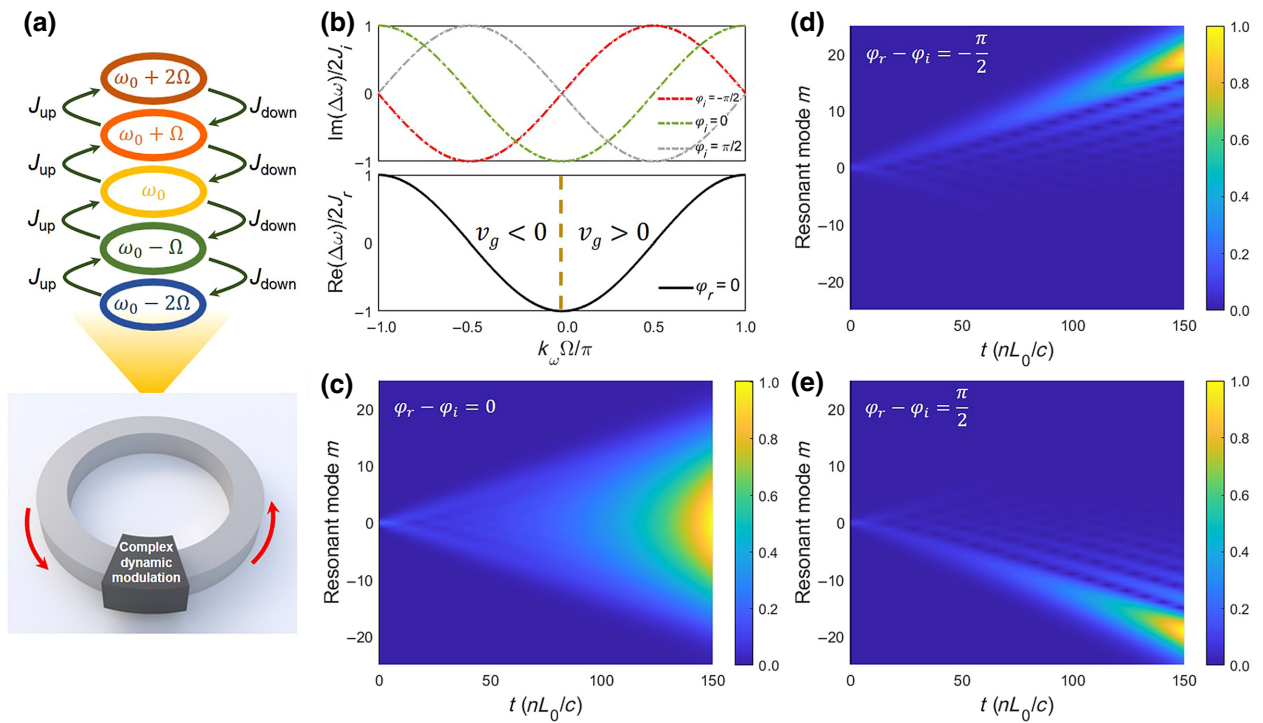


FIG. 2. 1D NHSE in synthetic frequency dimension. (a) Schematic for constructing the synthetic frequency dimension. (b) Real part (bottom) and imaginary part (top) of the band structure, respectively. Calculated spectrum evolution for different phase differences (c) $\varphi_r - \varphi_i = 0$, (d) $\varphi_r - \varphi_i = -\pi/2$, (e) $\varphi_r - \varphi_i = \pi/2$, when excited by a single-frequency light. The results in (c)–(e) are calculated by finite-difference approaches.

between two adjacent lattices. δ is a real number and represents the non-Hermitian coupling induced by gain and loss in the link rings. The corresponding non-Hermitian Hamiltonian in k space is written as

$$H_{k_z} = (\kappa + \delta)e^{-ik_z} + (\kappa - \delta)e^{ik_z} = 2\kappa \cos k_z - 2i\delta \sin k_z. \quad (2)$$

Figure 1(c) plots the eigenenergy solved in periodic boundary condition (PBC, red line) and open-boundary condition (OBC, black dots) respectively. The eigenenergy for the OBC lies in the eigenenergy for PBC, which indicates the non-Bloch bulk-boundary correspondence of the system [18]. For a 1D NHSE lattice, the decay lengths of all the modes can be calculated by $L_{\text{skin}} = 1/\{\log[(\kappa + \delta)/(\kappa - \delta)]\}^{1/2}\}$ [19]. For isotropic coupling ($\delta = 0$), the decay length L_{skin} tends to infinity, indicating that no eigenstate can be localized in the lattice. This prediction is well confirmed by the result in Fig. 1(d). While for the anisotropic coupling in the lattice ($\delta = 0.5\kappa$), the decay length is calculated to be $1/(\log\sqrt{3})$, suggesting that NHSE will appear in the photonic lattice. The directional flow of the light can also be well explained by the band structure in Fig. S1(b) within the Supplemental Material [46]. Furthermore, we create a lattice with an interface by flipping the direction of the anisotropy at some position, as illustrated in Fig. 1(e). In this situation,

the entire eigenmode spectrum collapses and all the eigenmodes are localized at the interface exponentially [Fig. 1(e)], representing a typical feature of the NHSE system.

A frequency dimension can be created by dynamic modulation of the complex refractive index, as illustrated in Fig. 2(a). The complex dynamic modulation is expressed as

$$n(t) = n_0 + n_r \cos(\Omega t + \varphi_r) + i n_i \cos(\Omega t + \varphi_i), \quad (3)$$

where n_0 is the background refractive index. Ω is the modulation frequency and is equal to the free spectral range of on-site rings. n_r and n_i are the modulated amplitude for the real and imaginary parts of the refractive index. φ_r and φ_i are the modulated phase for the real and imaginary parts, respectively. Since a ring resonator supports a series of discrete frequency modes, it can be considered to possess a synthetic dimension along the frequency axis [41], as depicted in Fig. 2(a). Here, we only take the coupling between the nearest-neighbor modes into account, and ignore the group velocity dispersion. Then, the non-Hermitian Hamiltonian of a single resonator can

be expressed as [34,47]

$$H_{\text{res}} = \sum_m [\omega_m a_m^\dagger a_m + 2J_r \cos(\Omega t + \varphi_r)(a_{m+1}^\dagger a_m + a_m^\dagger a_{m+1}) + 2iJ_i \cos(\Omega t + \varphi_i)(a_{m+1}^\dagger a_m + a_m^\dagger a_{m+1})], \quad (4)$$

where a_m^\dagger (a_m) is the creation (annihilation) operator for the m th mode. J_r and J_i refer to the amplitudes of the coupling strength between adjacent modes induced by the real part and the imaginary part of the modulation, respectively. After transformation by $c_m \equiv a_m \exp(-i\omega_m t)$ and rotating wave approximation, Eq. (4) can be written as

$$H_{\text{res}} = \sum_m (J_{\text{up}} c_{m+1}^\dagger c_m + J_{\text{down}} c_m^\dagger c_{m+1}), \quad (5)$$

$$J_{\text{up}} = J_r e^{i\varphi_r} + iJ_i e^{i\varphi_i}, \quad (6)$$

$$J_{\text{down}} = J_r e^{-i\varphi_r} + iJ_i e^{-i\varphi_i}, \quad (7)$$

where J_{up} and J_{down} are the coupling strengths for up-conversion and down-conversion, respectively.

The synthetic frequency dimension can support Bloch modes with $a_m(t) = \exp(imk_\omega) \exp(i\Delta\omega t)$, where k_ω and $\Delta\omega$ are the Bloch momentum of the frequency dimension and the eigenfrequency of the Hamiltonian in Eq. (5), respectively. Combining Eqs. (5)–(7), the band structure for the frequency dimension is obtained to be

$$\Delta\omega(k_w) = -2J_r \cos(k_w \Omega - \varphi_r) - 2iJ_i \cos(k_w \Omega - \varphi_i). \quad (8)$$

The real part of the band structure determines the trajectory of the frequency evolution by group velocity $v_g = \text{Re}(\partial\Delta\omega/\partial k_\omega)$. k_ω represents the fast time variable of light traveling in the ring resonator [48]. Thus, the imaginary part of the band structure indicates the time windows with gain or loss, which controls the energy evolution of the frequency comb [48–50].

To facilitate analysis, the real part (bottom) and the imaginary part (top) of the band structure are plotted in Fig. 2(b). The phase differences between the real part and the imaginary part of the dynamic modulation is tuned. For the cases $\varphi_r - \varphi_i = 0, \pm\pi$, the band structure is symmetric as $\Delta\omega(k_w \Omega) = \Delta\omega(-k_w \Omega)$, and $J_{\text{up}} = J_{\text{down}}$. Therefore, when all of the Bloch modes are excited with a single-frequency light, the up-conversion and the down-conversion of the frequency will take place symmetrically, which exactly coincides with the simulation result in Fig. 2(c). While for the cases $\varphi_r - \varphi_i \neq 0, \pm\pi$, the symmetry is broken as $\Delta\omega(k_w \Omega) \neq \Delta\omega(-k_w \Omega)$, and the anisotropic coupling will appear between the frequency modes ($J_{\text{up}} \neq J_{\text{down}}$). In Fig. 2(b), the Bloch momentum for $v_g > 0$ and $v_g < 0$ correspond to the time windows with

gain and loss ($\varphi_r - \varphi_i = -\pi/2$), respectively. As a result, the original center frequency of the incident light experiences up-conversion over time, which agrees well with the simulation result in Fig. 2(d). While for $\varphi_r - \varphi_i = \pi/2$ [Fig. 2(e)], the simulation result shows that the frequency experiences a down-conversion process, as the anisotropic coupling is reversed ($J_{\text{up}} < J_{\text{down}}$). However, when the group-velocity dispersion is considered, natural boundaries exist in the frequency space. Therefore, it is conceivable that the NHSE can be achieved in the frequency dimension by a dynamically modulated ring resonator with suitable phase difference ($\varphi_r - \varphi_i \neq 0, \pm\pi$).

As mentioned above, a 2D lattice can be constructed in the ring resonators with a synthetic frequency dimension. In Fig. 3, the dynamic modulation is applied to the ring resonator at the center of the array, thus realizing a synthetic 2D NHSE system with a single connected line. For convenience, the frequency mode for the incident light is set to be $m = 0$, and the modulated on-site ring (at the center of the lattice) is set as $n = 0$. Then, the non-Hermitian Hamiltonian of the 2D lattice is expressed as

$$H_{\text{array}} = \sum_m \left\{ \sum_n \omega_m a_{m,n}^\dagger a_{m,n} + \sum_{n<0} [(\kappa + \delta) a_{m,n+1}^\dagger a_{m,n} + (\kappa - \delta) a_{m,n}^\dagger a_{m,n+1}] \right. \\ \left. + \sum_{n \geq 0} [(\kappa - \delta) a_{m,n+1}^\dagger a_{m,n} + (\kappa + \delta) a_{m,n}^\dagger a_{m,n+1}] \right\} \\ + \sum_m \{ 2J_r \cos(\Omega t + \varphi_r)(a_{m+1,0}^\dagger a_{m,0} + a_{m,0}^\dagger a_{m+1,0}) \\ + 2iJ_i \cos(\Omega t + \varphi_i)(a_{m+1,0}^\dagger a_{m,0} + a_{m,0}^\dagger a_{m+1,0}) \}, \quad (9)$$

where the $a_{m,n}^\dagger$ ($a_{m,n}$) is the creation (annihilation) operator for the m th resonant mode at the n th on-site ring. After being transformed by $c_{m,n} \equiv a_{m,n} \exp(-i\omega_m t)$, Eq. (9) is written as

$$H_{\text{array}} = \sum_m \left\{ \sum_{n<0} [(\kappa + \delta) c_{m,n+1}^\dagger c_{m,n} + (\kappa - \delta) c_{m,n}^\dagger c_{m,n+1}] \right. \\ \left. + \sum_{n \geq 0} [(\kappa - \delta) c_{m,n+1}^\dagger c_{m,n} + (\kappa + \delta) c_{m,n}^\dagger c_{m,n+1}] \right\} \\ + \sum_m [J_r (e^{i\varphi_r} c_{m+1,0}^\dagger c_{m,0} + e^{-i\varphi_r} c_{m,0}^\dagger c_{m+1,0}) \\ + iJ_i (e^{i\varphi_i} c_{m+1,0}^\dagger c_{m,0} + e^{-i\varphi_i} c_{m,0}^\dagger c_{m+1,0})]. \quad (10)$$

Since the 2D system in this work does not have translation invariance in the spatial dimension, we can just introduce Bloch wavevector k_ω in the synthesized frequency

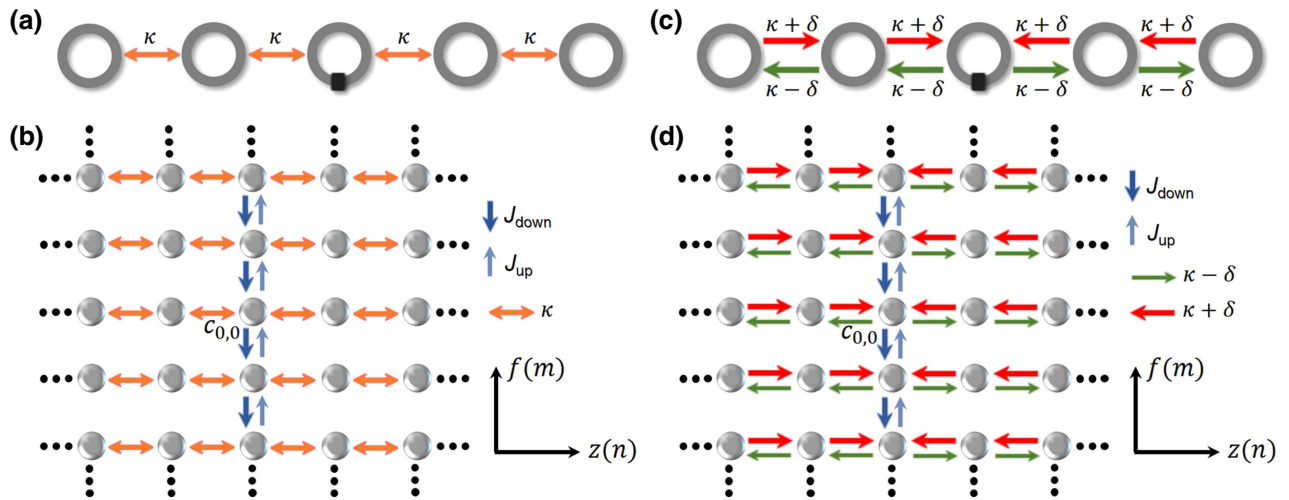


FIG. 3. Constructing a 2D NHSE lattice by combining the spatial dimension and the synthetic frequency dimension. (a) Schematic diagram of a lattice with isotropic coupling in space. The complex refractive index of the on-site ring at the center of the array is modulated dynamically. (b) The corresponding schematic diagram for the 2D lattice synthesized with the model in (a). (c) Schematic diagram of a lattice composed of two lattices with opposite anisotropic coupling. The complex refractive index of the on-site ring at the center of the array is modulated dynamically. (d) The corresponding schematic diagram for the 2D lattice synthesized with the model in (c).

dimension. Therefore, to obtain the energy evolution of the incident light in the synthesized frequency dimension, OBC and PBC are imposed to the spatial dimension and the frequency dimension, respectively. We assume that the 2D lattices are constituted by 61 on-site rings (the 31st on-site ring is modulated), and the frequencies of the modes are off resonance for $|m| > 20$. The corresponding non-Hermitian Hamiltonian in k_ω space is written as

$$H_{k_\omega}^{\text{array}} = \sum_{n=-30}^{-1} [(\kappa + \delta)a_{k_\omega, n+1}^\dagger a_{k_\omega, n} + (\kappa - \delta)a_{k_\omega, n}^\dagger a_{k_\omega, n+1}] \\ + \sum_{n=0}^{29} [(\kappa - \delta)a_{k_\omega, n+1}^\dagger a_{k_\omega, n} + (\kappa + \delta)a_{k_\omega, n}^\dagger a_{k_\omega, n+1}] \\ + [2J_r \cos(k_\omega \Omega - \varphi_r) a_{k_\omega, 0}^\dagger a_{k_\omega, 0} \\ + 2iJ_i \cos(k_\omega \Omega - \varphi_i) a_{k_\omega, 0}^\dagger a_{k_\omega, 0}]. \quad (11)$$

The band structures for $\delta = 0$ and $\delta = 0.5\kappa$ are, respectively, plotted in Figs. S2 and S3 within the Supplemental Material [46], which indicate that the frequency will experience a directional up-conversion, a symmetrical conversion and a directional down-conversion for $\varphi_r - \varphi_i = -\pi/2$, 0 , $\pi/2$, respectively.

In order to demonstrate the prediction, the energy evolution and distribution in the synthetic lattice are calculated. Firstly, we consider the situation that the coupling between two adjacent on-site rings is isotropic ($\delta = 0$), as shown in Fig. 3(a). The corresponding schematic diagram of the 2D lattice is exhibited in Fig. 3(b). In this case, when a

single-frequency light is incident from the leftmost on-site ring, the light flows back and forth in the photonic lattice, resulting in a wide distribution in space [Figs. 4(a)–4(c)]. When the light reaches the on-site ring with dynamic modulation, the frequency conversion takes place. In Fig. 4(a) ($\varphi_r - \varphi_i = -\pi/2$) and Fig. 4(c) ($\varphi_r - \varphi_i = \pi/2$), the original center frequency of the light can be, respectively, converted to higher frequency and lower frequency, which results from the anisotropic coupling between the adjacent frequency modes and agrees well with the predictions in Fig. S2 (Supplemental Material [46]). The outcomes indicate that the first-order NHSE along the frequency dimension appears in the 2D synthetic photonic lattice. While for $\varphi_r - \varphi_i = 0$, the coupling between the adjacent frequency modes is isotropic, which leads to a symmetric frequency conversion, as shown in Fig. 4(b).

However, the situation becomes different when the anisotropic coupling is introduced between the two adjacent on-site rings by adding gain and loss into the link rings ($\delta = 0.5\kappa$). In Figs. 4(c) and 4(d), the lattice is formed by two lattices with opposite anisotropic coupling. As mentioned in Fig. 1(e), the anisotropic coupling in the spatial dimension will induce NHSE in real space, and drive all the modes of light flow to the interface of the lattice. The results in Figs. 4(d)–4(f) confirm that when the leftmost on-site ring is excited with a single-frequency light, the light flows to the interface unidirectionally. As a result, the light can be localized at the interface exponentially, as labeled by yellow arrows. As the light arrives at the interface, frequency conversion will happen in the on-site ring at the interface, as labeled by white arrows. In Fig.

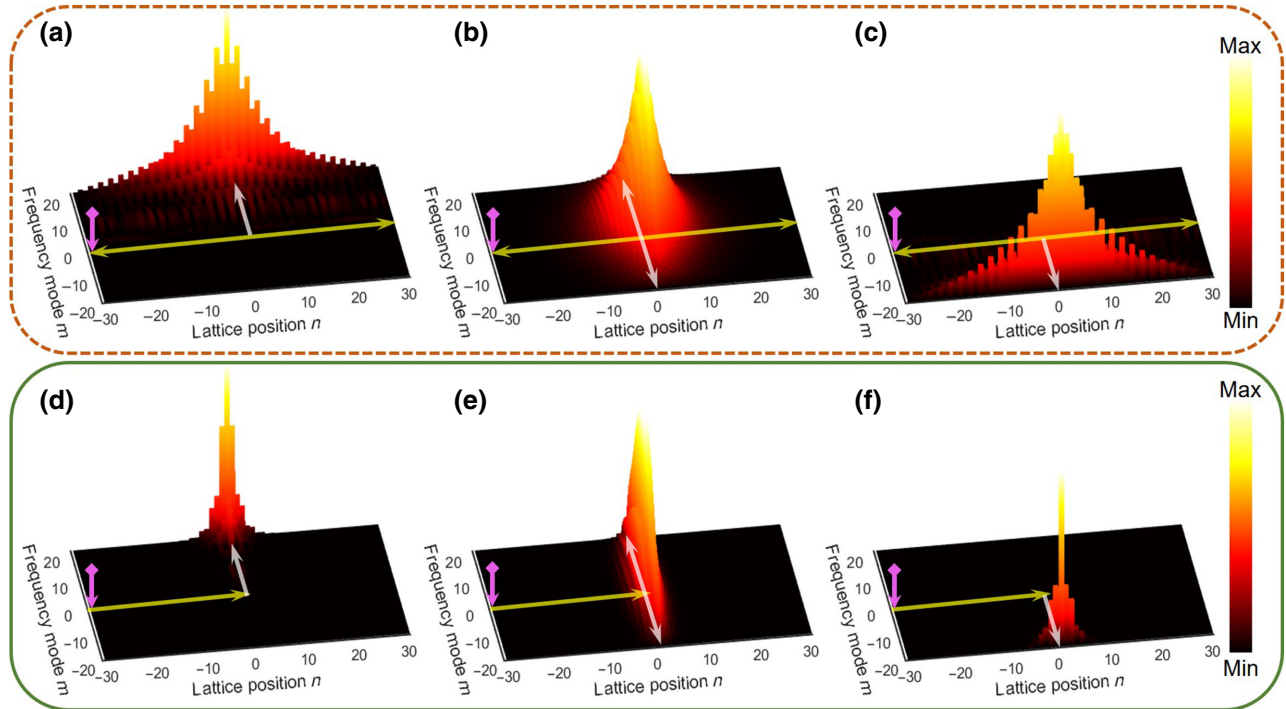


FIG. 4. Calculated light evolutions and distributions in the synthetic 2D photonic lattices (61×41 sites). (a)–(c) The calculated results for the 2D lattice with isotropic coupling in space [Fig. 3(b)]. When a single-frequency light is incident from the leftmost on-site ring, the light flows back and forth in the lattice and has a wide distribution in space. The center frequency of the light experiences (a) an up-conversion for $\varphi_r - \varphi_i = -\pi/2$, (b) a symmetric conversion for $\varphi_r - \varphi_i = 0$, and (c) a down-conversion for $\varphi_r - \varphi_i = \pi/2$, respectively. (d)–(f) The calculated results for the 2D lattice with anisotropic coupling in space [Fig. 3(d)]. When a single-frequency light is incident from the leftmost on-site ring, the light flows to the interface unidirectionally. The center frequency of the light experiences (d) an up-conversion for $\varphi_r - \varphi_i = -\pi/2$, (e) a symmetric conversion for $\varphi_r - \varphi_i = 0$, and (f) a down-conversion for $\varphi_r - \varphi_i = \pi/2$, respectively.

4(d), the center frequency of the incident light experiences an up-conversion for $\varphi_r - \varphi_i = -\pi/2$. And then, the frequency mode is localized at the boundary of the synthetic frequency dimension due to the group-velocity dispersion, which agrees with the frequency conversion predicted by the band structures in Fig. S3 (Supplemental Material [46]). Overall, the incident light can be localized both in the spatial dimension and the frequency dimension exponentially, which behaves like a 2D NHSE system with second-order corner skin modes. The opposite frequency conversion is observed for $\varphi_r - \varphi_i = \pi/2$ [Fig. 4(f)], as the anisotropic coupling between frequency modes is reversed. While for $\varphi_r - \varphi_i = 0$ [Fig. 4(e)], the frequency modes experience a symmetric conversion, due to the isotropic coupling in frequency domain. As a result, the lattice acts like a first-order NHSE system. Moreover, once we stop the dynamic modulation, the longitudinal coupling between the frequency modes will disappear, and we can obtain a stable frequency distribution of the light in the 2D photonic lattice. To summarize, the synthetic 2D lattice can realize the 2D NHSE with first-order and second-order skin modes by controlling the coupling in the spatial dimension and the synthetic frequency dimension

simultaneously, which would enable programmable light propagation and frequency conversion.

In addition, the anisotropic coupling will protect the skin modes of the NHSE system from disturbances in the lattice [45]. In order to confirm, the robustness of the 2D NHSE system is explored, as shown in Fig. 5. For the spatial dimension, disorder and point defect are introduced into the coupling of the ring-resonator array, respectively. The disorder will induce a long-range interference effect (Anderson localization), and it can be suppressed by NHSE [13]. To demonstrate, Fig. 5(a) presents the result for a uniformly distributed gain-loss disorder $\Delta\delta \in [-W, W]$, $W = 0.48$. We can observe that the light can overcome the long-range interference to flow to the interface. As a result, the frequency can still experience an up-conversion ($\varphi_r - \varphi_i = -\pi/2$), which demonstrates an excellent robust of the 2D NHSE against the coupling disorder. Similarly, the constructed 2D NHSE is also immune to the point defect [Fig. 5(b)], except that the coupling is completely blocked by the defect [Fig. 5(c)]. For the frequency dimension, the disorder is created by introducing a uniformly distributed phase differences $\Delta\varphi \in [-Q, Q]$. Figures 5(d)–5(f) display the light evolutions for

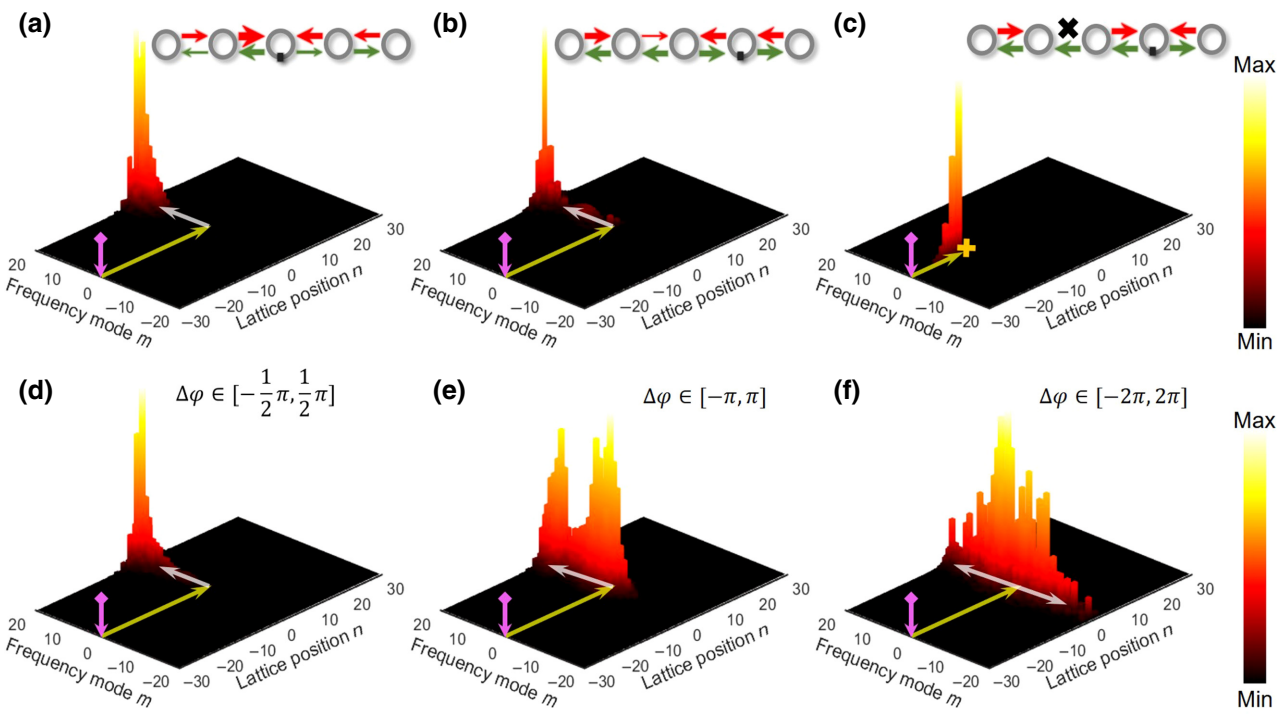


FIG. 5. Robustness for the synthetic 2D NHSE lattice. (a)–(c) Robustness of the 2D NHSE lattice in the spatial dimension. Calculated light distribution with (a) a gain-loss disorder, (b) a point defect with greatly weakened coupling ($\delta = -0.9 \kappa$), and (c) a point defect with blocked coupling, respectively. (d)–(e) Robustness of the synthetic 2D NHSE lattice in the frequency dimension. The disorder is created by introducing a uniformly distributed phase differences between the real part and imaginary part of the complex refractive index of the ring resonator, $\varphi_r - \varphi_i = -\pi/2 + \Delta\varphi$, $\Delta\varphi \in [-Q, Q]$. Calculated light distribution for (d) $Q = \pi/2$, (e) $Q = \pi$, and (f) $Q = 2\pi$, respectively.

the condition of $\varphi_r - \varphi_i = -\pi/2 + \Delta\varphi$. For $Q = \pi/2$, the single-frequency light incident from the leftmost ring can flow to the interface, and experience a frequency up-conversion [Fig. 5(d)], which is nearly the same as the result for $\Delta\varphi = 0$ (no disorder). For a stronger disorder ($Q = \pi$), the frequency mode can also experience an up-conversion, indicating that the anisotropic coupling in frequency dimension is still kept [Fig. 5(e)]. For a completely random distribution of the phase difference ($Q = 2\pi$), the anisotropic coupling no longer exists in the frequency dimension, and the directional frequency conversion will be destroyed [Fig. 5(f)]. Overall, the 2D NHSE lattice has an excellent robustness both in the spatial dimension and the frequency dimension.

Finally, we focus on the realization of the 2D NHSE system in practice. In experiment, optical gain and loss has been introduced into the optical system by selectively pumping optically active materials, which can be applied for introducing the anisotropic coupling in the ring-resonator array [3,6,51]. Meanwhile, the complex refractive index of the ring resonators can be modulated by utilizing the electro-optic effect [33,52,53] and nonlinear Kerr effect [54,55], with an ultrafast response, which has become a good candidate for realizing the synthetic frequency dimension. Therefore, the 2D NHSE system can be

conveniently realized by optical integration, which shows great promise for developing ultrafast and functional optoelectronic devices on chip.

III. CONCLUSIONS

In conclusion, we construct a 2D NHSE photonic lattice in a 1D ring-resonator array, by combining the spatial dimension and a synthetic frequency dimension. The anisotropic couplings in the spatial dimension and frequency dimension are realized by introducing gain and loss and dynamically modulating the complex refractive index, respectively. The synthetic 2D NHSE system enables us to manipulate the position and frequency mode of the light in real time, leading to programmable light propagation and frequency conversion. We also demonstrate that the incident light can be localized in the spatial dimension and the frequency dimension separately or simultaneously, which correspond to the first-order and second-order skin modes in the synthetic 2D lattice, respectively. Besides, the 2D NHSE system exhibits an excellent robustness for the disorder and point defect in the lattice. We emphasize that the introduction of gain and loss and dynamical modulation in the optical system have been widely studied in experiment, indicating that the 2D NHSE system can be conveniently

realized by optical integration. This work generalizes the concept of non-Hermitian skin effect in synthetic dimension, which will inspire versatile platforms to investigate the non-Hermitian photonics and related light-matter interactions in multiple dimensions. Moreover, the 2D non-Hermitian skin effect in the synthetic lattice enables us to realize programmable light propagation and frequency conversion, which shows great promise for potential applications in on-chip light manipulation, frequency synthesis, and information processing.

ACKNOWLEDGMENTS

This work is supported by the National Natural Science Foundation of China (Grants No. 11804109, No. 11204097, and No. 11674117).

- [1] L. Pan, X. Chen, Y. Chen, and H. Zhai, Non-Hermitian linear response theory, *Nat. Phys.* **16**, 767 (2020).
- [2] S. Ke, D. Zhao, J. Liu, Q. Liu, Q. Liao, B. Wang, and P. Lu, Topological bound modes in anti-PT-symmetric optical waveguide arrays, *Opt. Express* **27**, 13858 (2019).
- [3] H. Zhao, X. Qiao, T. Wu, B. Midya, S. Longhi, and L. Feng, Non-Hermitian topological light steering, *Science* **365**, 1163 (2019).
- [4] H.-Z. Chen, T. Liu, H.-Y. Luan, R.-J. Liu, X.-Y. Wang, X.-F. Zhu, Y.-B. Li, Z.-M. Gu, S.-J. Liang, H. Gao, L. Lu, L. Ge, S. Zhang, J. Zhu, and R.-M. Ma, Revealing the missing dimension at an exceptional point, *Nat. Phys.* **16**, 571 (2020).
- [5] M. A. Miri and A. Alu, Exceptional points in optics and photonics, *Science* **363**, eaar7709 (2019).
- [6] S. K. Ozdemir, S. Rotter, F. Nori, and L. Yang, Parity-time symmetry and exceptional points in photonics, *Nat. Mater.* **18**, 783 (2019).
- [7] X. Han, K. Wang, P. D. Persaud, X. Xing, W. Liu, H. Long, F. Li, B. Wang, M. R. Singh, and P. Lu, Harmonic resonance enhanced second-harmonic generation in the monolayer WS₂-Ag nanocavity, *ACS Photonics* **7**, 562 (2020).
- [8] L. Xiao, T. Deng, K. Wang, G. Zhu, Z. Wang, W. Yi, and P. Xue, Non-Hermitian bulk-boundary correspondence in quantum dynamics, *Nat. Phys.* **16**, 761 (2020).
- [9] Z. Fedorova, H. Qiu, S. Linden, and J. Kroha, Observation of topological transport quantization by dissipation in fast thouless pumps, *Nat. Commun.* **11**, 3758 (2020).
- [10] K. Y. Bliokh, D. Leykam, M. Lein, and F. Nori, Topological non-Hermitian origin of surface Maxwell waves, *Nat. Commun.* **10**, 580 (2019).
- [11] K. Kawabata, K. Shiozaki, M. Ueda, and M. Sato, Symmetry and Topology in Non-Hermitian Physics, *Phys. Rev. X* **9**, 041015 (2019).
- [12] T. Biesenthal, M. Kremer, M. Heinrich, and A. Szameit, Experimental Realization of PT-Symmetric Flat Bands, *Phys. Rev. Lett.* **123**, 183601 (2019).
- [13] S. Weidemann, M. Kremer, T. Helbig, T. Hofmann, A. Stegmaier, M. Greiter, R. Thomale, and A. Szameit, Topological funneling of light, *Science* **368**, 311 (2020).
- [14] Q. Liu, C. Qin, B. Wang, and P. Lu, Scattering singularities of optical waveguides under complex modulation, *Phys. Rev. A* **101**, 033818 (2020).
- [15] S. A. Hassani Gangaraj and F. Monticone, Topological Waveguiding Near an Exceptional Point: Defect-Immune, Slow-Light, and Loss-Immune Propagation, *Phys. Rev. Lett.* **121**, 093901 (2018).
- [16] X. W. Luo and C. Zhang, Higher-Order Topological Corner States Induced by Gain and Loss, *Phys. Rev. Lett.* **123**, 073601 (2019).
- [17] Z. Yang, E. Lustig, G. Harari, Y. Plotnik, Y. Lumer, M. A. Bandres, and M. Segev, Mode-Locked Topological Insulator Laser Utilizing Synthetic Dimensions, *Phys. Rev. X* **10**, 011059 (2020).
- [18] N. Okuma, K. Kawabata, K. Shiozaki, and M. Sato, Topological Origin of Non-Hermitian Skin Effects, *Phys. Rev. Lett.* **124**, 086801 (2020).
- [19] C. H. Lee, L. Li, and J. Gong, Hybrid Higher-Order Skin-Topological Modes in Nonreciprocal Systems, *Phys. Rev. Lett.* **123**, 016805 (2019).
- [20] C. H. Lee and R. Thomale, Anatomy of skin modes and topology in non-Hermitian systems, *Phys. Rev. B* **99**, 201103(R) (2019).
- [21] K. Zhang, Z. Yang, and C. Fang, Correspondence Between Winding Numbers and Skin Modes in Non-Hermitian Systems, *Phys. Rev. Lett.* **125**, 126402 (2020).
- [22] K. Kawabata, M. Sato, and K. Shiozaki, Higher-order non-Hermitian skin effect, (2020), <https://arxiv.org/abs/2008.03721>.
- [23] S. Longhi, Stochastic non-Hermitian skin effect, *Opt. Lett.* **45**, 5250 (2020).
- [24] L. Li, C. H. Lee, and J. Gong, Topological Switch for Non-Hermitian Skin Effect in Cold-Atom Systems with Loss, *Phys. Rev. Lett.* **124**, 250402 (2020).
- [25] L. Li, C. H. Lee, S. Mu, and J. Gong, Critical non-Hermitian skin effect, *Nat. Commun.* **11**, 5491 (2020).
- [26] F. Song, S. Yao, and Z. Wang, Non-Hermitian Skin Effect and Chiral Damping in Open Quantum Systems, *Phys. Rev. Lett.* **123**, 170401 (2019).
- [27] F. K. Kunst, E. Edvardsson, J. C. Budich, and E. J. Bergholtz, Biorthogonal Bulk-Boundary Correspondence in Non-Hermitian Systems, *Phys. Rev. Lett.* **121**, 026808 (2018).
- [28] R. Okugawa, R. Takahashi, and K. Yokomizo, Second-order topological non-Hermitian skin effects, (2020), <https://arxiv.org/abs/2008.03721>.
- [29] O. Zilberberg, S. Huang, J. Guglielmon, M. Wang, K. P. Chen, Y. E. Kraus, and M. C. Rechtsman, Photonic topological boundary pumping as a probe of 4D quantum Hall physics, *Nature* **553**, 59 (2018).
- [30] L. J. Maczewsky, K. Wang, A. A. Dovgiy, A. E. Miroshnichenko, A. Moroz, M. Ehrhardt, M. Heinrich, D. N. Christodoulides, A. Szameit, and A. A. Sukhorukov, Synthesizing multi-dimensional excitation dynamics and localization transition in one-dimensional lattices, *Nat. Photonics* **14**, 76 (2019).
- [31] Q. Wang, K. Ding, H. Liu, S. Zhu, and C. T. Chan, Exceptional cones in 4D parameter space, *Opt. Express* **28**, 1758 (2020).
- [32] E. Lustig, S. Weimann, Y. Plotnik, Y. Lumer, M. A. Bandres, A. Szameit, and M. Segev, Photonic topological

- insulator in synthetic dimensions, *Nature* **567**, 356 (2019).
- [33] A. Dutt, Q. Lin, L. Yuan, M. Minkov, M. Xiao, and S. Fan, A single photonic cavity with two independent physical synthetic dimensions, *Science* **367**, 59 (2020).
- [34] L. Yuan, Y. Shi, and S. Fan, Photonic gauge potential in a system with a synthetic frequency dimension, *Opt. Lett.* **41**, 741 (2016).
- [35] Q. Lin, X. Q. Sun, M. Xiao, S. C. Zhang, and S. Fan, A three-dimensional photonic topological insulator using a two-dimensional ring resonator lattice with a synthetic frequency dimension, *Sci. Adv.* **4**, eaat2774 (2018).
- [36] X. W. Luo, X. Zhou, J. S. Xu, C. F. Li, G. C. Guo, C. Zhang, and Z. W. Zhou, Synthetic-lattice enabled all-optical devices based on orbital angular momentum of light, *Nat. Commun.* **8**, 16097 (2017).
- [37] L. Yuan, Q. Lin, A. Zhang, M. Xiao, X. Chen, and S. Fan, Photonic Gauge Potential in One Cavity with Synthetic Frequency and Orbital Angular Momentum Dimensions, *Phys. Rev. Lett.* **122**, 083903 (2019).
- [38] H. Chalabi, S. Barik, S. Mittal, T. E. Murphy, M. Hafezi, and E. Waks, Guiding and confining of light in a two-dimensional synthetic space using electric fields, *Optica* **7**, 506 (2020).
- [39] H. Chalabi, S. Barik, S. Mittal, T. E. Murphy, M. Hafezi, and E. Waks, Synthetic Gauge Field for Two-Dimensional Time-Multiplexed Quantum Random Walks, *Phys. Rev. Lett.* **123**, 150503 (2019).
- [40] A. Dutt, M. Minkov, I. A. D. Williamson, and S. Fan, Higher-order topological insulators in synthetic dimensions, *Light.: Sci. Appl.* **9**, 131 (2020).
- [41] A. Dutt, M. Minkov, Q. Lin, L. Yuan, D. A. B. Miller, and S. Fan, Experimental band structure spectroscopy along a synthetic dimension, *Nat. Commun.* **10**, 3122 (2019).
- [42] A. Dutt, M. Minkov, Q. Lin, L. Yuan, D. A. B. Miller, and S. Fan, Experimental demonstration of dynamical input isolation in nonadiabatically modulated photonic cavities, *ACS Photonics* **6**, 162 (2018).
- [43] X. Zhu, H. Wang, S. K. Gupta, H. Zhang, B. Xie, M. Lu, and Y. Chen, Photonic non-hermitian skin effect and non-Bloch bulk-boundary correspondence, *Phys. Rev. Res.* **2**, 013280 (2020).
- [44] M. Hafezi, E. A. Demler, M. D. Lukin, and J. M. Taylor, Robust optical delay lines with topological protection, *Nat. Phys.* **7**, 907 (2011).
- [45] N. Hatano and D. R. Nelson, Localization Transitions in Non-Hermitian Quantum Mechanics, *Phys. Rev. Lett.* **77**, 570 (1996).
- [46] See Supplemental Material at for <http://link.aps.org/supplemental/10.1103/PhysRevApplied.14.064076> band structures of the synthetic photonic lattice.
- [47] L. Yuan and S. Fan, Bloch oscillation and unidirectional translation of frequency in a dynamically modulated ring resonator, *Optica* **3**, 1014 (2016).
- [48] L. Yuan, Q. Lin, M. Xiao, A. Dutt, and S. Fan, Pulse shortening in an actively mode-locked laser with parity-time symmetry, *APL Photonics* **3**, 086103 (2018).
- [49] C. Qin, B. Wang, Z. J. Wong, S. Longhi, and P. Lu, Discrete diffraction and Bloch oscillations in non-Hermitian frequency lattices induced by complex photonic gauge fields, *Phys. Rev. B* **101**, 064303 (2020).
- [50] S. Ke, Q. Liu, D. Zhao, and W. Liu, Spectral discrete diffraction with non-Hermitian coupling, *J. Opt. Soc. Am. B* **35**, 2387 (2018).
- [51] W. Liu, M. Li, R. S. Guzzon, E. J. Norberg, J. S. Parker, M. Lu, L. A. Coldren, and J. Yao, An integrated parity-time symmetric wavelength-tunable single-mode microring laser, *Nat. Commun.* **8**, 15389 (2017).
- [52] C. Qin, F. Zhou, Y. Peng, D. Sounas, X. Zhu, B. Wang, J. Dong, X. Zhang, A. Alu, and P. Lu, Spectrum Control Through Discrete Frequency Diffraction in the Presence of Photonic Gauge Potentials, *Phys. Rev. Lett.* **120**, 133901 (2018).
- [53] M. Zhang, B. Buscaino, C. Wang, A. Shams-Ansari, C. Reimer, R. Zhu, J. M. Kahn, and M. Loncar, Broadband electro-optic frequency comb generation in a lithium niobate microring resonator, *Nature* **568**, 373 (2019).
- [54] S. Yu, X. Wu, K. Chen, B. Chen, X. Guo, D. Dai, L. Tong, W. Liu, and Y. Ron Shen, All-optical graphene modulator based on optical Kerr phase shift, *Optica* **3**, 541 (2016).
- [55] M. Pu, L. Ottaviano, E. Semenova, and K. Yvind, Efficient frequency comb generation in AlGaAs-on-insulator, *Optica* **3**, 823 (2016).